Journal of Advanced Concrete Technology
Materials, Structures and Environment

Effect of stirrups on the shear failure mechanism of deep beams

Yasar Hanifi Gedik, Hikaru Nakamura, YoshihitoYamamot, Naoshi Ueda, Minoru Kunieda
Journal of Advanced Concrete Technology, volume 10 (2012), pp. 14-30

Related Papers Click to Download full PDF!

Seismic Capacity Requirements for Low-Rise Reinforced Concrete Buildings Controlled by both Shear and Flexure
Kang Seok Lee
Journal of Advanced Concrete Technology, volume 8 (2010), pp. 75-91

Local Stress Filed Approach for Shear Failure Assessment of Reinforced Concrete Members
Masoud Soltani, Bahman Ghiassi
Journal of Advanced Concrete Technology, volume 8 (2010), pp. 223-238

Modeling and Analysis of Shear-Critical ECC Members with Anisotropic Stress and Strain Fields
Benny Suryanto, Kohei Nagai, Koichi Maekawa
Journal of Advanced Concrete Technology, volume 8 (2010), pp. 239-258

Influence of Longitudinal Bar Corrosion on Shear Behavior of RC beams
Xue Xin, Hiroshi Seki
Journal of Advanced Concrete Technology, volume 8 (2010), pp. 145-156

Smeared-Crack Modeling of R/ECC Membranes Incorporating an Explicit Shear Transfer Model
Benny Suryanto, Kohei Nagai, Koichi Maekawa
Journal of Advanced Concrete Technology, volume 8 (2010), pp. 315-326

Click to Submit your Papers
Japan Concrete Institute http://www.j-act.org

Scientific paper

Effect of Stirrups on the Shear Failure Mechanism of Deep Beams

Yasar Hanifi Gedik[1], Hikaru Nakamura[2], Yoshihito Yamamoto[3], Naoshi Ueda[4] and Minoru Kunieda[5]

Received 11 June 2011, accepted 14 November 2011 doi:10.3151/jact.10.14

Abstract

The purpose of this study is to clarify the effect of stirrups in deep beams by investigating the shear failure mechanism analytically by using the 3-D Rigid-Body-Spring Model analytical tool. The investigation of the analytical results of the internal stress state and 3-D deformations of deep beams were the key objectives of this study. Firstly, the applicability of the analytical tool on deep beams was confirmed by comparison of analytical and experimental results. Then, the stirrup contribution to load carrying capacity of deep beams was investigated and the shear failure mechanism based on the B and D region concept was clarified analytically. To achieve this, analytical results such as stress distribution, 3-D deformations, crack patterns and strain of stirrups were investigated. Three types of stirrup effect were observed in deep beams. In the a/d= 0.5 case, the peak load increase due to the confinement effect of stirrups. In the a/d=1.0 case, the stirrup contributes to the strut action that leads to an increase in load. In the case of $a/d < 1.0$, the D region is dominant. On the other hand, the peak load increases significantly with increases of stirrup ratio in the case of $a/d > 1.5$, in which the truss analogy is dominant rather than the strut action.

1. Introduction

The shear failure mechanism of RC deep beams differs from that of ordinary beams and several studies thus far have investigated the shear failure mechanism and shear strength of deep beams (Zararis 2003; Yang *et al*. 2003; Ashour 2000; Tan *et al*. 1999; Sanad *et al*. 2001; Salamy *et al*. 2005; Tang *et al*. 2004; Mau *et al*. 1989; Ashour *et al*. 2003; Rogowsky *et al*. 1986; Smith *et al*. 1982; Wang *et al*. 1993; Averbuch *et al*. 1999). In deep beams, a considerable amount of the load is carried by compression struts and the strain distribution in the member is considered as non-linear (MacGregor 1997). Moreover, the effect of stirrups is limited for smaller shear span to depth ratios (a/d) (Kosa *et al*. 2005; Tanimura *et al*. 2004). Therefore, the evaluation of shear strength of deep beams is more complicated and requires a deep comprehension of the load carrying mechanism and a different evaluation method than that used for slender beams.

The conventional way to evaluate the shear strength of RC beams is to add up the concrete contribution (Vc) and the stirrup contribution (Vs) calculated using a truss model, which is a basic tool for the analysis and design of RC concrete beams. Truss models were first proposed by Ritter (1899), and then Mörsch (1920, 1922) applied truss models for torsion. In 1987, the strut-and-tie model (STM) approach, which is extended from truss models for beams and is particularly convenient for deep beams, was introduced by Schlaich *et al*. (1987). That work introduced the concept of the B and D regions, where B means beam or Bernoulli regions, in which plane sections remain plane, and D means discontinuity or disturbed regions, where the assumption of the plane sections remaining plane is inappropriate (ASCE-ACI Committee 445 1998). That is, a linear strain distribution forms in B regions whereas the strain distribution is nonlinear in D regions. In beams, the whole member becomes a D region when the a/d ratio is small. STM is particularly convenient for the design of D regions that have a complex internal stress state (ASCE-ACI Committee 445 1998).

In ACI 318-0.5 Code (ACI 2005), the limit shear span to height ratio (a_v/h) is given as two for deep beams, which can be considered as a single D region for design, and STM can be used for the design of the D regions.

On the other hand, a method to calculate the shear strength of deep beams is given by Eq. 1 in The Standard Specifications for Concrete Structures (JSCE 2002). In this method, stirrup contribution is calculated based on the truss analogy and the calculated value is then reduced depending on the a/d ratio. That is, the stirrup effect decreases for smaller a/d ratios. However, in the JSCE's 2007 Specifications (JSCE 2007), the previous method was revised based on the experimental results. The new method is given in Eq. 2, in which the effect of stirrups is determined based on the increase of concrete

[1]PhD, Department of Civil Engineering, Nagoya University, Japan.
E-mail:hanifigedik@msn.com
[2]Professor, Department of Civil Engineering, Nagoya University, Japan.
[3]Assistant Professor, Department of Civil & Environmental Engineering, National Defense Academy Kanagawa, Japan.
[4]Assistant Professor, Department of Civil Engineering, Nagoya University, Japan.
[5]Associate Professor, Department of Civil Engineering, Nagoya University, Japan.

contribution. The stirrup effect increases through increases of the stirrup ratio (p_{wb}) and shear span to depth ratio (a_v/d) parameters.

$$V_{ydd} = V_{cdd} + V_{sdd} \quad (1)$$

$$V_{cdd} = \beta_d . \beta_p . \beta_a . f_{dd} . b_w . d / \gamma_b \quad (1.a)$$

$$f_{dd} = 0.19\sqrt{f'_{cd}} \ , \ (\mathrm{N/mm^2}) \quad (1.b)$$

$$\beta_d = \sqrt[4]{1000/d} \ , \ \text{when } \beta_d > 1.5, \beta_d \text{ shall be } 1.5 \quad (1.c)$$

$$\beta_p = \sqrt[3]{100 p_w} \ , \text{when } \beta_p > 1.5, \beta_p \text{ shall be } 1.5 \quad (1.d)$$

$$\beta_a = \frac{5}{1+(a_v/d)^2} \quad (1.e)$$

$$V_{sdd} = \varphi \ . \ V_{sd} \quad (1.f)$$

$$\varphi = -0.17 + 0.3(a_v/d) + 0.33/p_{wb} \leq 1.0 \quad (1.g)$$

$$V_{sd} = [A_w . f_{wyd} \ (\sin\alpha_s + \cos\alpha_s)/s_s + A_{pw} . \sigma_{pw} \ (\sin\alpha_p + \cos\alpha_p)/s_p] z/\gamma_b \quad (1.h)$$

where;

V_{ydd} : Design shear capacity
b_w : Web width
γ_b : This value shall generally be 1.3
f'_{cd} Design compressive strength of concrete ($\mathrm{N/mm^2}$)
d : Effective depth (mm)
p_w : Longitudinal tension reinforcement ratio (%)
a_v : Shear span
V_{sdd} : Design shear strength of stirrup in accordance with Eq. 1.f
V_{sd} : Contribution of shear strength computed with Eq. 1.h
p_{wb} : Stirrup ratio (%)

$$V_{cdd} = (\beta_d + \beta_w) . \beta_p . \beta_a . f_{dd} . b_w . d / \gamma_b \quad (2)$$

$$\beta_w = 4.2\sqrt[3]{100 p_{wb}} . (a/d - 0.75)/\sqrt{f'_{cd}} \quad (2.a)$$

$$\beta_p = \frac{1+\sqrt{100 p_w}}{2}, \text{ when } \beta_p > 1.5, \beta_p \text{ shall be } 1.5 \quad (2.b)$$

where V_{cdd} is the design shear capacity and β_d, β_a and f_{dd} are the same values as those given in Eq. 1. γ_b shall generally be 1.2. Different approaches in design codes show that the shear strength of deep beams is not yet fully understood.

Beside the design codes, in the literature, several studies investigate the contribution of stirrups to the shear strength of deep beams (Kosa *et al*. 2005 and 2006; Tanimura *et al*. 2004; Mau *et al*. 1987; Tan *et al*. 1997). However, the effect of stirrups on the load carrying capacity and shear failure mechanism of deep beams has not been fully clarified yet.

In this study, the effect of stirrups on the shear failure mechanism of RC deep beams due to shear span to depth ratio (*a/d*) was investigated analytically. It is known that the shear capacity of deep beams strongly depends on the *a/d* ratio. The purpose was to investigate different shear failure mechanism of deep beams with stirrups from small *a/d* ratios to larger ones and to clarify the mechanisms depending on *a/d* ratios. The analytical tool used was 3-D RBSM (Rigid-Body-Spring Model), which is a representative example of the discrete element method and was first proposed by Kawai (Kawai 1978; Bolander *et al*. 2000, 2002; Saito 1999). RBSM can show realistic behavior of concrete structures from cracking to failure. It can also be used to investigate stress transfer mechanisms at the meso-level. Furthermore, 3-D behavior as well as the effects of confinement of concrete can be simulated by 3-D RBSM (Yamamoto 2010; Gedik *et al*. 2011).

To demonstrate the applicability of 3-D RBSM on deep beams, a series of deep beams with and without stirrups and *a/d* values ranging from 0.5 to 2.0 was tested. The tested specimens were also analyzed by 3-D RBSM. The experimental and analytical results were compared and the simulation capability of the analytical tool was confirmed. Then, beam series with *a/d* values ranging from 0.5 to 3.0 were analyzed by 3-D RBSM. The stirrup contribution to the load carrying capacity and the shear failure mechanism based on the B and D region concept was investigated in detail by evaluation of load-displacement curves, crack pattern, 3-D deformations, strut behavior and stress distribution, crack widths and the strain of stirrups. The key objectives of this study were the analytical investigation of the internal stress state and 3-D deformations. As a result, the beams with *a/d* values ranging from 0.5 to 3.0 were classified into three different groups based on the shear failure mechanism and *a/d* ratio.

2. Analytical model

2.1 3-D RBSM

RBSM was proposed first by Kawai (1978). In this model, a concrete member is designed as an assemblage of rigid particles linked by springs located at their boundaries. The spring model provides the response of interaction among particles, unlike models based on continuum mechanics. Three translational and three rotational degrees of freedom are defined for each particle at the nucleus, which indicates the center of the particle (**Fig. 1.a**). As seen in the figure, the interface of two particles is partitioned into several triangles with a center of gravity and vertices. One normal and two tangential springs are defined at the integral point, which represents the center of the triangles. The effect of bending and torsional moment can be automatically evaluated in this model without setting any rotational springs since a rotation can be calculated by using the coordinates of two integral points (Yamamoto *et al*. 2008, Yamamoto 2010).

The mesh design strongly affects the crack pattern since the cracks initiate and propagate along the boundary interface of particles. In order to reduce the mesh dependency of crack development, a random geometry of rigid particles is produced by means of a Voronoi diagram (**Fig. 1.b**) (Bolander *et al*. 2000).

2.2 Concrete material model

Figure 2 shows the constitutive models for tension, compression and shear that are used in 3-D RBSM (Yamamoto *et al*. 2008). The tensile model of normal spring is given in **Fig. 2.a**. The tensile behavior of concrete is assumed as linear elastic up to tensile strength, and a bilinear softening branch according to a ¼ model is considered after cracking. Tensile fracture energy is taken into consideration in the model. In the figure, h, σ_t and g_f indicate distance between nuclei, tensile strength and tensile fracture energy, respectively.

The stress-strain relation for compression of normal springs is given in **Fig. 2.b**. **Table 1** gives the parame-

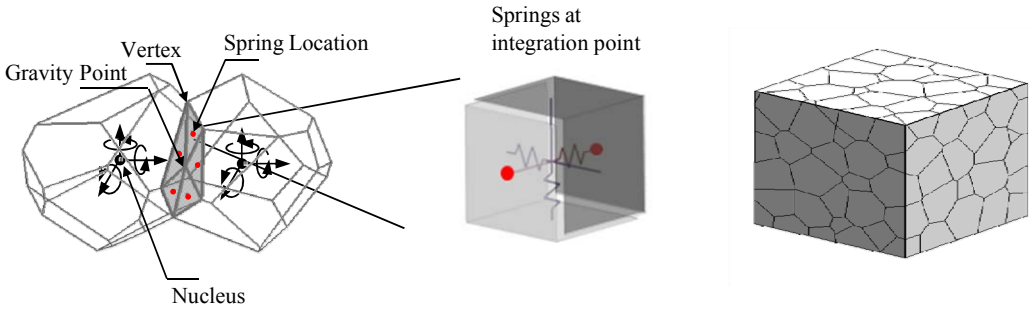

Fig. 1 a) Rigid-Body-Spring model b) Voronoi diagram.

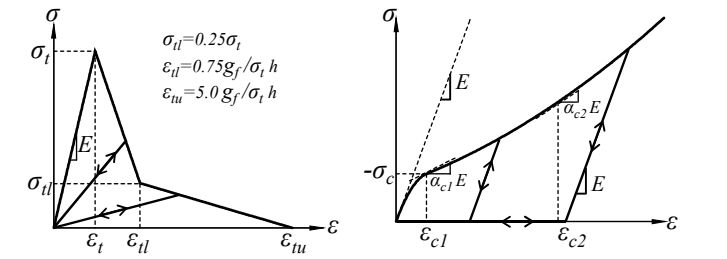

a) Tensile Model of Normal Spring

b) Compression Model of Normal Spring

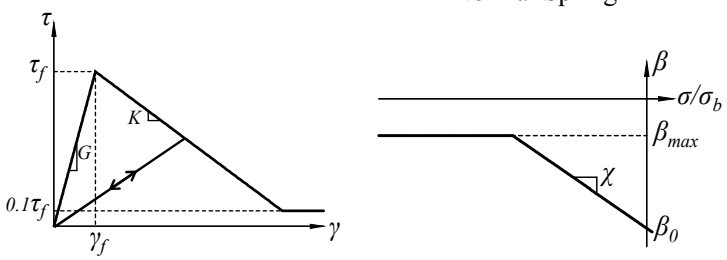

c) Shear Spring Model

d) Softening Coefficient for Shear Spring

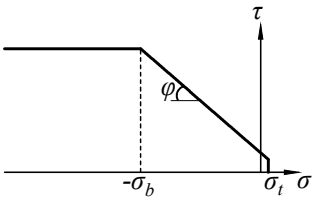

e) Mohr-Coulomb Criteria

Fig. 2 Concrete Constitutive Models (Yamamoto *et al*. 2008).

Table 1 Model parameters (Yamamoto 2010).

Normal Spring							Shear Spring							
Young Modulus	Tensile Area		Compressive Area				Young Modulus	Fracture Criterion			Softening Behavior			
E (N/mm^2)	σ_t (N/mm^2)	g_f (N/mm^2)	σ_c (N/mm^2)	ε_{c2}	α_{c1}	α_{c2}	$\eta=G/E$	c (N/mm^2)	Φ (degree)	σ_b (N/mm^2)	β_0	β_{max}	χ	κ
E*	0.80f_t*	0.5G_f*	1.5f_c'*	-0.015	0.15	0.25	0.35	0.14f_c'*	37	f_c'*	-0.05	-0.025	-0.01	-0.3

" *" indicates the experimental values. E*:Young Modulus, f_t*: Tensile Strength, G_f*: Fracture Energy, f_c'*:Compressive Strength

ters of constitutive models. The parameters were determined by performing parametric analyses and comparing the results with the test results for uniaxial compression and tension, triaxial compression and hydrostatic compression including many specimens with various specimen size and strength (Yamamoto 2010). Softening behavior is not considered and compressive failure of normal springs does not take place in this model. However, the model simulates the compressive failure behavior by a confinement effect through a combination of normal and shear springs (Yamamoto 2010).

The combination of two tangential springs is represented in the stress-strain relation of shear stress. Equation 3 defines the combined shear strain, where γ_l and γ_m indicate the strains of the springs in two directions (Nagai *et al*. 2005). Therefore, combined shear stress τ is obtained from the shear stress-strain relation and the shear stresses for each direction (τ_l and τ_m) are calculated as given in Eq. 4.

$$\gamma = \sqrt{\gamma_l^2 + \gamma_m^2} \tag{3}$$

$$\tau_l = \tau(\gamma_l/\gamma),\ \tau_m = \tau(\gamma_m/\gamma) \tag{4}$$

Figure 2.c shows the stress-strain relationship for shear where τ_f and γ_f indicate shear strength and strain corresponding to strength, respectively. Up to the shear strength, the stress elastically increases with the slope of shear modulus (G). In the softening part, K is the shear-softening coefficient and it is described by Eq. 5. The shear-softening coefficient K is assumed to be due to the stress of the normal spring as defined in **Fig. 2.d**. In the figure, β_{max} , β_0 and χ are normal spring dependent parameters for the shear-softening coefficient. (Yamamoto *et al*. 2008).

$$K=\beta.G \tag{5}$$

Figure 2.e shows the Mohr-Coulomb criterion that is considered as the failure criteria for the shear spring. The parameters of c and φ represent the cohesion and the angle of internal friction, respectively. In the figure, σ_b is termed the compression limit value and when normal stress is greater than σ_b , shear strength is assumed to be constant (Yamamoto 2010).

The model can consider dilatancy since random mesh geometry is generated by using a voronoi diagram rather than a regular mesh design. That is, the dilatancy can be captured by occurrence of slip at the inclined interfaces of particles (Yamamoto 2010).

It is noted that the model parameters given above are recommended for the average size of voronoi particles from 10 mm to 30 mm and for normal strength concrete (Yamamoto 2010). The average size of the voronoi particles used in the analysis was 20 mm for all cases in this study.

2.3 Reinforcement model

Figure 3 shows the reinforcement model, which is formed as a series of regular beam elements that can simulate the bending effects. In this model, the reinforcement can be freely positioned within the member, regardless of the mesh design of concrete (Bolander *et al*. 2002). At each beam node, two translational and one rotational degree of freedom are defined by means of the springs. The reinforcement is attached to the concrete particles by zero-size link elements, which provide a load-transfer mechanism between a concrete particle and a beam node (Saito 1999). A bi-linear model is assumed for the stress-strain relation of reinforcement. The bond interaction between concrete and reinforce-

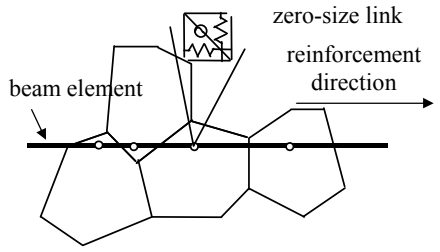

Fig. 3 Reinforcement arrangement.

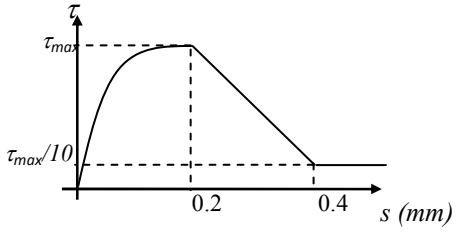

Fig. 4 Bond stress-slip relation.

ment strongly affects crack development. The spring parallel to the reinforcement of the linked element provides the bond stress-slip relation, which is given in **Fig. 4**. The relation is defined by Eq. 6 up to τ_{max} (Suga *et al*. 2001), and after the strength τ_{max}; the relation proposed by CEB-FIB is considered (CEB 1990),

$$\tau = 0.36 f_c'^{2/3} \left\{ 1 - \exp\ (-40(s/D)^{0.5}) \right\} \quad (6)$$

where s represents slippage and D is the diameter of the reinforcement.

The simulation capability of confinement by reinforcement is given by Gedik *et al*. (2011) and Yamamoto (2010) by comparison of the uniaxial compression test of Akiyama *et al*. (2004) and 3-D RBSM simulation of Yamamoto (2010). An example of confined concrete is given here. The details of the specimen are shown in **Figs. 5.a** and **5.b** and **Table 2**. The comparison of the stress-strain relationship for the specimen between the analysis and experimental results is given in **Fig. 5.c**. As seen in that figure, both the compressive strength of confined concrete and post-peak behavior agree significantly well, which confirms the simulation capability of the model for confined concrete.

3. Experimental program

Four groups of deep beams with a/d=0.5, 1.0, 1.5 and 2.0 as described in **Table 3** were designed and tested. Each group had two beams with and without stirrup. The dimensions and details of the specimens are given in **Fig. 6**. The plate width was 100 mm in each specimen. The cross-sectional area, longitudinal reinforcement ratio (ρ_t) and plate widths were the same in all cases.

Four-point loading was applied to the test specimens. The load was distributed to the bearing plates using a steel beam. Steel rollers were used between the loading plates and the steel beam. A mid-span and support deflections were measured and the relative mid-span deflection was taken into consideration by subtracting the support displacements. In the experiment, strain gauges, the locations of which are labeled as 'G1' and 'G2'in **Fig. 6**, were attached to the stirrups in order to measure the strain values.

4. Experimental and analytical results

The tested beams described in Section 3 were also simulated by 3-D RBSM, which can give realistic behavior from cracking to failure. Moreover, 3-D RBSM can also be used to investigate the stress-transfer mechanism at the meso levels (Yamamoto *et al*. 2008, Yamamoto 2010). Furthermore, it is applicable to the simulation of uniaxial tension, uniaxial compression, localized compressive failure as well as 3-D effects, the triaxial stress state, dilatancy and confinement effect, which have been investigated in several studies (Yamamoto 2010, Gedik *et al*. 2010). 3-D RBSM can simulate multiaxial behavior as well as the confinement effect provided by stirrups (Gedik 2011). Moreover, the applicability of 3-D

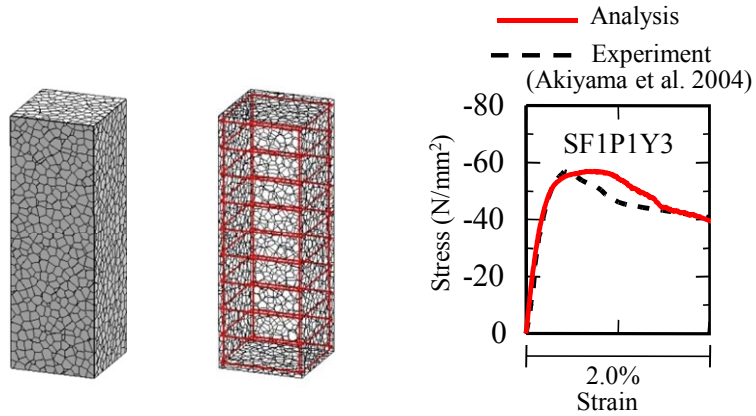

Fig. 5 Analytical model and stress-strain relationship (Yamamoto 2010).

Table 2 Stirrup properties (Yamamoto 2010).

Specimen No.	Properties of stirrup				Concrete Strength
	Diameter	Space	Volumetric ratio	Yield strength	
	mm	mm	%	MPa	Mpa
SF1P1Y3	6.4	25	1.92	1288	46.3

Table 3 Specimens details.

Specimen	a/d	Effective Depth d (mm)	Shear Span a (mm)	Longitudinal Reinforcement			Stirrup				Compressive Strength fc' (MPa)	Peak Loads (kN)	
				As (mm^2)	fy (N/mm^2)	ρ_t (%)	Type	fyw (N/mm^2)	Spacing (mm)	ρ_w (%)		Experimental	Analytical
B3-0.5	0.5	240	120	774.2 (2D22)	372.2	3.23	-	388.2	-	-	32.6	601	662
B3-0.5-VS	0.5	240	120				D6	388.2	70	0.9	32.6	658	598
B3-1.0	1.0	240	240				-	388.2	-	-	35.7	452	402
B3-1.0-VS	1.0	240	240				D6	388.2	70	0.9	35.7	465	470
B3-1.5	1.5	240	360				-	388.2	-	-	22.2	209	193
B3-1.5-VS	1.5	240	360				D6	388.2	70	0.9	22.2	274	294
B3-2.0	2.0	240	480				-	388.2	-	-	22.2	130	146
B3-2.0-VS	2.0	240	480				D6	388.2	70	0.9	22.2	221	256

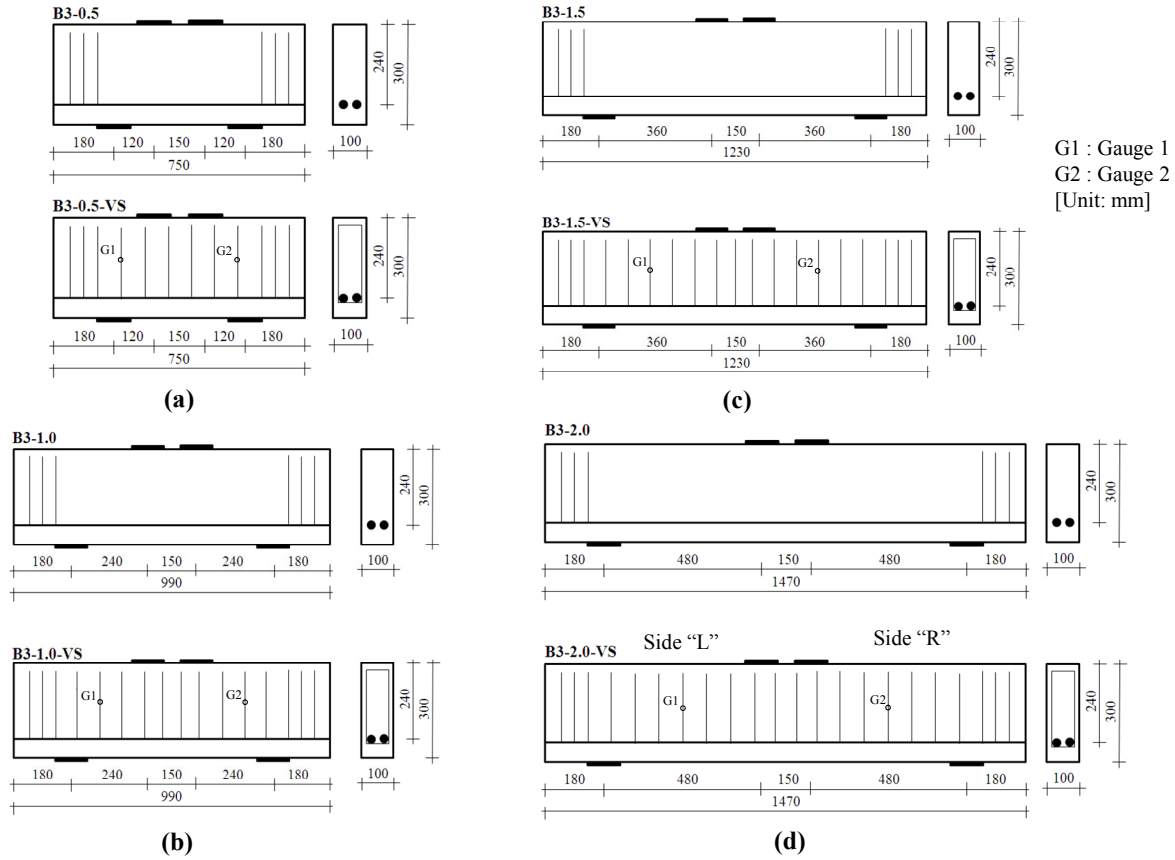

Fig. 6 Overview of specimens.

RBSM to deep beams is confirmed in this section by comparing the experimental and analytical results in terms of the load-displacement curves, crack patterns and strain of the stirrups.

The experimental and analytical results for each series are given as follows.

4.1 *a/d*=0.5 case

The experimental and the analytical load-displacement curves for B3-0.5 and B3-0.5-VS are given in **Fig. 7**, and the peak load values are listed in **Table 3**. In the experiment, the peak load decreases in the B3-0.5-VS case. This may be due to the reduction of the effective beam width caused by stirrup arrangement since the width of the specimen is small. On the other hand, this effect is not considered in the analysis and the analytical peak load increases in the B3-0.5-VS specimen compared to the B3-0.5 case. The reason will be discussed in Section 5.

The comparison of the experimental and analytical crack patterns of B3-0.5 and B3-0.5-VS is shown in **Fig. 8**. The crack patterns are given in two steps: at shear

cracking propagation at the pre-peak of P=500 kN (labeled 'a' and 'A' for the experiment and the analysis, respectively) and at the peak load (b, B). In this section, the analytical crack pattern figures are magnified by a factor (M.F.) that is indicated in each figure. In the experiment, the crack pattern is similar in both the B3-0.5 and B3-0.5-VS cases. That is, there is no significant effect of the stirrups on the crack pattern. On the other hand, the analytical results agree significantly well with the experimental ones for B3-0.5 and B3-0.5-VS as seen in the figure.

Figure 9 shows the comparison of stirrup strains between the analysis and the experiment for the B3-0.5-VS specimen. The strain measurement locations in the experiment are labeled as 'G1' and 'G2'in **Fig. 6** in Section 3. On the other hand, the analytical strain is given in the range of the one-third to two-third height of the stirrups at several points rather than only at the middle height of the stirrups, since the strain values are influenced by the crack location. Since the reinforcement is modeled by several small beam elements, the average size of which is the same as the average mesh size of concrete, the local strain values of stirrups can be obtained by evaluation of strain at a local beam element. The indices 'L' and 'R' represent the two sides of the beam that are also labeled in **Fig. 6**. The same procedure is also used for analytical strain curves of B3-1.0-VS, B3-1.5-VS and B3-2.0-VS in this section. As seen in **Fig. 9**, reasonable agreement between the experiment and the analysis is observed even in the post-peak region. That is, the strain values in both experiment and analysis are negative in the pre-peak region and then become positive in the post-peak region. Moreover, the strain values are similar in the experiment and the analysis. On the other hand, the difference between the analytical strain values in the given range is small. This means that localization of damage on a crack having a large width does not occur and that the strut behavior is dominant around the shear crack.

4.2 *a/d*=1.0 case

The comparison of the analytical and experimental load-displacement curves for B3-1.0 and B3-1.0-VS are given in **Fig. 10**. In the experiment, B3-1.0 and B3-1.0-VS show similar behavior as seen in the figure. On the other hand, the analytical peak load increases in B3-1.0-VS compared to the B3-1.0 case. The analytical peak load of B3-1.0 is lower than the experimental one. However, it is similar with the shear strength equation of Niwa (1983), which is also labeled in the figure. Moreover, the initial stiffness is larger in the analysis; however, it agrees with the theoretical value calculated by the Timoshenko beam theory.

The comparison of the experimental and the analytical crack patterns for the B3-1.0 and B3-1.0-VS cases is given in **Fig. 11**. In the experiment, the number of shear cracks slightly increases on both shear spans in B3-1.0-VS due to the stirrup effect. The B3-1.0 specimen sud-

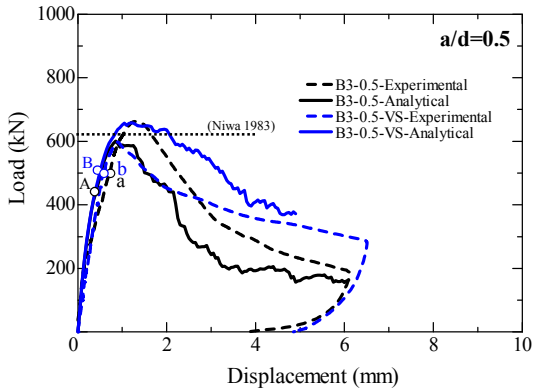

Fig. 7 Load displacement curve (a/d=0.5).

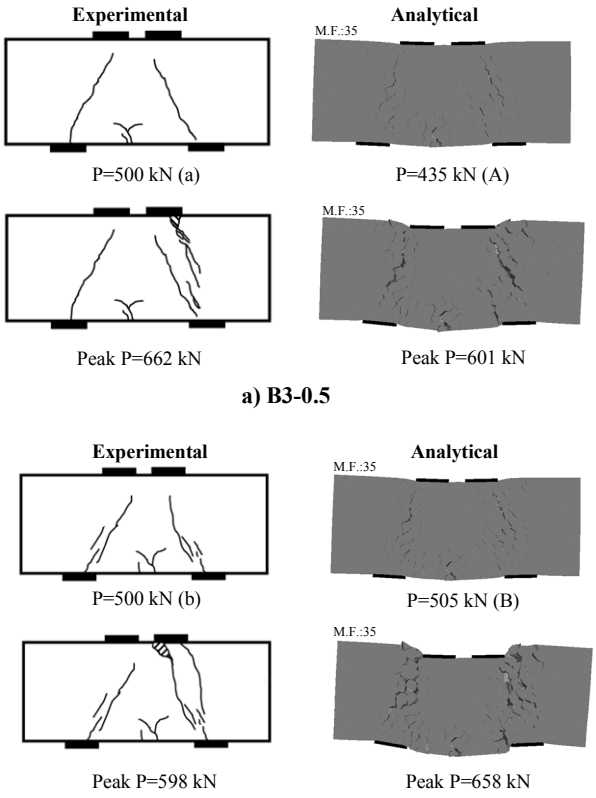

Fig. 8 Crack pattern (a/d=0.5).

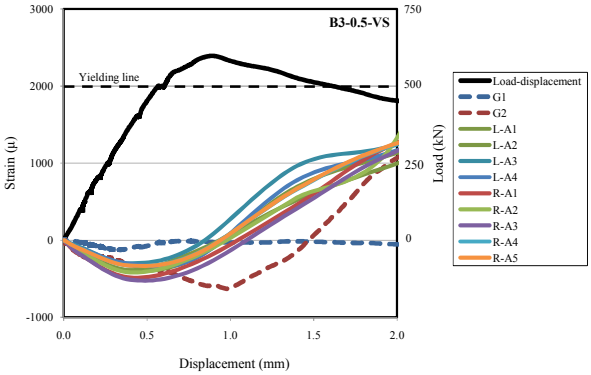

Fig. 9 Strain of stirrups (B3-0.5-VS).

denly failed in the shear compression and shear compression failure occurred in the B3-1.0-VS case. In the analysis, several shear cracks occurred on one of the shear spans of the beam, whereas only one main crack occurred on the other shear span of B3-1.0 specimen that is similar with the experiment. On the other hand, several shear cracks were observed on both shear spans due to the stirrup effect in the B3-1.0-VS case. Thus good agreement between the analytical and experimental crack pattern and failure modes was obtained.

The comparison of stirrup strain between the analysis and the experiment for the B3-1.0-VS specimen is given in **Fig. 12**. Similarly with the experimental results, stirrups did not yield before the peak in the analysis. Moreover, the analytical results agree significantly well with the experimental results. Comparing the strain range on side "R", the range of strain values on side "L" is expanded since the failure occurred on this side. However, the range is still relatively small, that is the strut behavior is also dominant around the shear crack for the *a/d*=1.0 case, which is similar with the *a/d*=0.5 case.

4.3 *a/d*=1.5 case

The experimental and the analytical load-displacement curves for B3-1.5 and B3-1.5-VS are given in **Fig. 13**. In the experiment, the peak load and the ductility increase significantly in the B3-1.5-VS case due to the effect of the stirrups. In the analysis, more brittle behavior and a smaller peak load are observed in the B3-1.5 case compared to the experimental one. However, the analytical peak load agrees with the shear strength equation of Niwa (1983) as demonstrated. Similarly with the experimental results, the load and ductility increase in the analysis of B3-1.5-VS. The analytical and the experimental curves for B3-1.5 and B3-1.5-VS agree reasonably well in both the pre-peak and post-peak regions as seen in the figure.

The comparison of the analytical and experimental crack patterns for B3-1.5 and B3-1.5-VS is given in **Fig. 14**. In the experiment, the damage was localized on the one main diagonal shear crack in the B3-1.5 case and a sudden diagonal shear failure occurred. On the other hand, several shear cracks occurred at the peak in the B3-1.5-VS case and more ductile behavior was observed due to the stirrups. That is, the stirrups led to several finer shear cracks rather than one main large crack and therefore more energy was absorbed and the load and ductility increased in the B3-1.5-VS case. In the analysis, only one shear crack occurred on the one shear span of the beam where more than one shear crack occurred on the other shear span in the B3-1.5 case. On the other hand, several shear cracks in both shear spans formed in the B3-1.5-VS specimen. Similarly with the experimental results, the beam suddenly failed in diagonal shear in the B3-1.5 case where diagonal shear failure with softening behavior was observed in the B3-1.5-VS specimen in the analysis.

Figure 15 shows the comparison of stirrup strains between the analysis and the experiment for the B3-1.5-VS specimen. The yielding of stirrups before the peak load is observed in both experiment and analysis. The analytical results reasonably agree with the experimen-

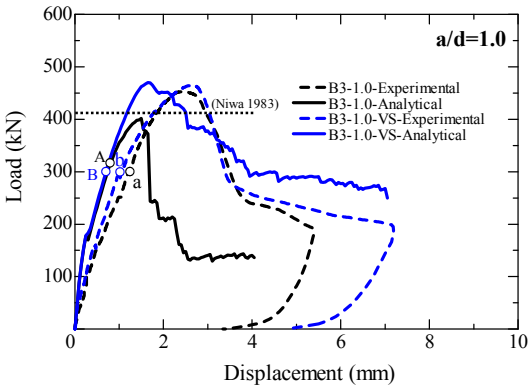

Fig. 10 Load displacement curve (a/d=1.0).

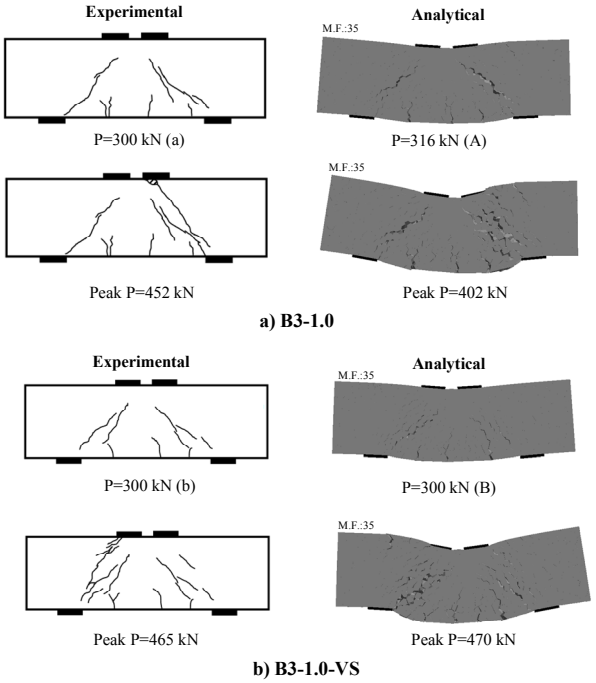

Fig. 11 Crack pattern (a/d=1.0).

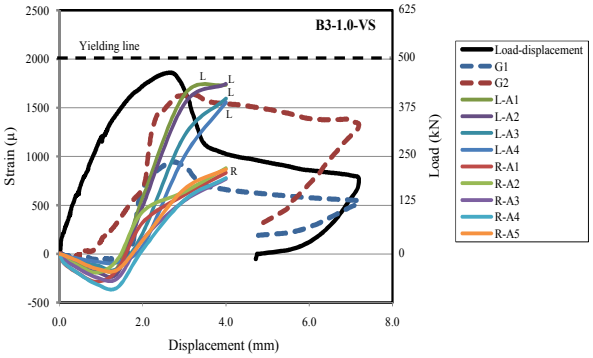

Fig. 12 Strain of stirrups (B3-1.0-VS).

tal results as seen in the figure. In the analysis, there is a wide range of strain values both on the "L" and "R" sides. The reason is that, since the damage is localized mainly in one diagonal crack direction, larger strain values are observed near the main diagonal crack. Therefore, the effect of the diagonal crack is dominant rather than the strut action.

4.4 *a/d*=2.0 case

Figure 16 shows the experimental and the analytical load-displacement curves for the B3-2.0 and B3-2.0-VS specimens. In the experiment and analysis, the peak load and the ductility increase significantly in the B3-2.0-VS case. The analytical and the experimental results agree well in both cases.

Figure 17 shows the comparison of the analytical and experimental crack patterns for B3-2.0 and B3-2.0-VS. In both the experiment and the analysis, the damage localizes on one main diagonal shear crack that leads to a sudden diagonal shear failure in the B3-2.0 case. On the other hand, several finer shear cracks occurred at the peak in the B3-2.0-VS case and more ductile behavior was observed. As seen in the figure, the crack patterns between the experiment and the analysis agreed significantly well in both the B3-2.0 and B3-2.0-VS cases. Moreover, the failure modes of B3-2.0 and B3-2.0-VS are the same in the analysis and experiment.

Figure 18 shows the comparison of stirrup strains between the analysis and the experiment for the B3-2.0-VS specimen. Yielding of the stirrups before the peak load is observed in the experiment and the analysis. The experimental and the analytical strain values are similar as seen in **Fig. 18**. On the other hand, the range of strain values on the "R" side, in which the failure occurs, is significantly wide. This confirms that the effect of diagonal crack is dominant in this case similarly with the *a/d*=1.5 case.

The comparison of the analytical and the experimental results show that 3-D RBSM can simulate deep beam behavior such as load-displacement curves, crack patterns and strain of stirrups significantly well. Moreover, 3-D RBSM can also simulate local and micro behavior as well as macro behavior. Thus, the simulation capability of the 3-D RBSM analytical method is confirmed.

5. Effect of stirrups on the shear failure mechanism

In this section, the effect of stirrups on the shear failure mechanism and load carrying capacity of deep beams are investigated in detail and the occurrence of the B and D regions in the beams are clarified. In order to achieve this, a number of beams were designed and analyzed. The specimen details are given in **Table 4**. The overview of the specimens for *a/d*=0.5, 1.0, 1.5 and 2.0 is the same as that given in **Fig. 6** in Section 3. However, the compressive strength of concrete (*fc'*) was set to 25 Mpa for all the specimens in this section. Moreover,

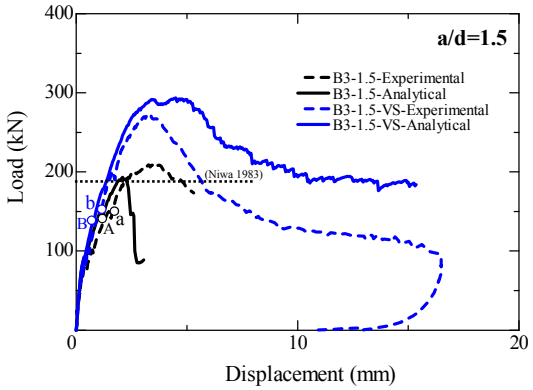

Fig. 13 Load displacement curve (a/d=1.5).

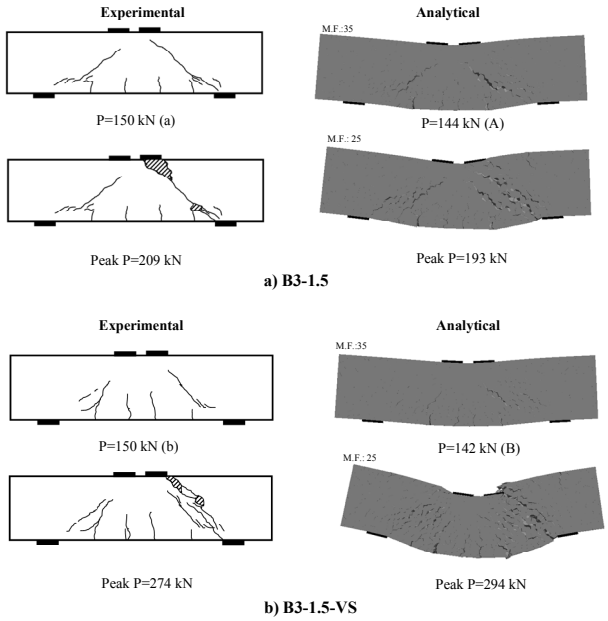

Fig. 14 Crack pattern (a/d=1.5).

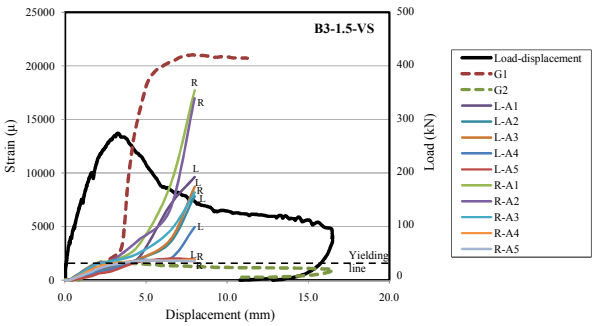

Fig. 15 Strain of stirrups (B3-1.5-VS).

specimens with *a/d*=3.0 were also analyzed in order to demonstrate the difference between deep beams and slender beams. Three specimens were analyzed for each *a/d* ratio, including the no stirrup case and the cases with stirrup ratios of ρ_w=0.45% and ρ_w=0.9%. However, the beam with ρ_w = 0.9% in the *a/d*=3.0 case was not included because flexural failure was observed.

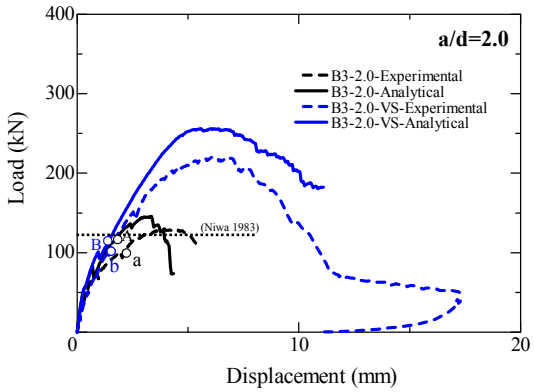

Fig. 16 Load displacement curve (a/d=2.0).

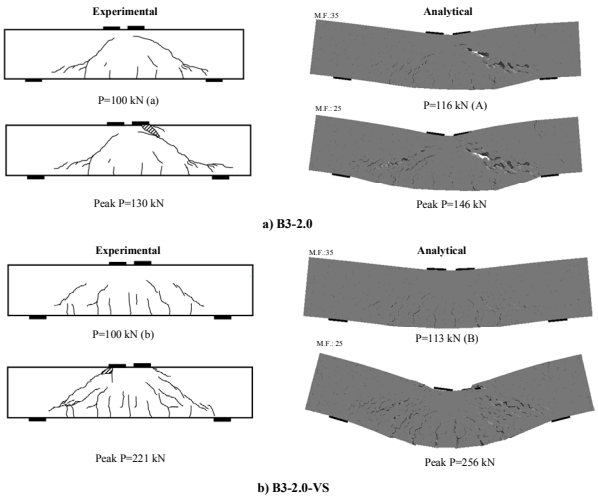

Fig. 17 Crack pattern (a/d=2.0).

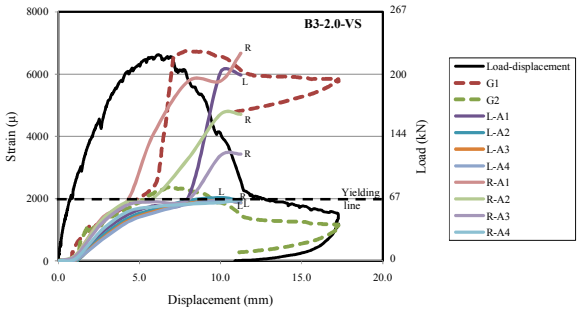

Fig. 18 Strain of stirrups (B3-2.0-VS).

Figure 19.a shows the comparison of the shear forces (*Vc*) between the analysis that is the results of the no stirrup cases and the equation of Niwa (1983). On the other hand, **Figure 19.b** gives the comparison of the shear force provided by the arrangement of stirrups (*Vs* = *V*-*Vc*). That is, the stirrup contribution (*Vs*) is obtained by subtracting the concrete contribution (*Vc*) from the total shear strength (*V*). Vs is given for the analytical results of beams with stirrups as well as the results calculated by truss analogy for both the ρ_w = 0.9% and ρ_w = 0.45% cases due to the *a/d* ratio.

Figure 19.b may be divided into three regions based on the shear failure mechanism and the stirrup contribution to the load carrying capacity. In the region where *a/d* is less than 1.0, the value of *Vs* increase as the a/d ratio decreases. This region is defined as Region 1. From *a/d*=0.5 to 1.0, the stirrup effect (*Vs*) decreases and its smallest value occurs in the vicinity of a/d=1.0. Then, *Vs* increases again up to *a/d*=2.0. The effect of the stirrups becomes significant for *a/d*=1.5 and 2.0. Therefore, the region from *a/d*=1.0 to 2.0 is defined as Region 2. After *a/d*=2.0, which is defined as Region 3, *Vs* is almost constant and it does not depend on the *a/d* ratio, which agrees with the results obtained from the truss analogy. The effect of stirrups for each region is discussed in detail below.

5.1 Region 1

5.1.1 *a/d*=0.5 case

The load displacement curves of B3-0.5, B3-0.5-VS and B3-0.5-VS (0.45%) are given in **Fig. 20**. The load and ductility increase in the beams with stirrups, however

Table 4 Specimen details.

Specimen	a/d	Shear Span a (mm)	Stirrup		Compressive Strength fc' (MPa)	Peak Loads (kN)
			Spacing (mm)	ρ_w (%)		
B3-0.5	0.5	120	-	-	25.0	522
B3-0.5-VS	0.5	120	70	0.9	25.0	594
B3-0.5-VS (0.45%)	0.5	120	70	0.45	25.0	568
B3-1.0	1.0	240	-	-	25.0	331
B3-1.0-VS	1.0	240	70	0.9	25.0	376
B3-1.0-VS (0.45%)	1.0	240	70	0.45	25.0	359
B3-1.5	1.5	360	-	-	25.0	203
B3-1.5-VS	1.5	360	70	0.9	25.0	296
B3-1.5-VS (0.45%)	1.5	360	70	0.45	25.0	257
B3-2.0	2.0	480	-	-	25.0	150
B3-2.0-VS	2.0	480	70	0.9	25.0	260
B3-2.0-VS (0.45%)	2.0	480	70	0.45	25.0	232
B3-3.0	3.0	720	-	-	25.0	91
B3-3.0-VS (0.45%)	3.0	720	70	0.45	25.0	157

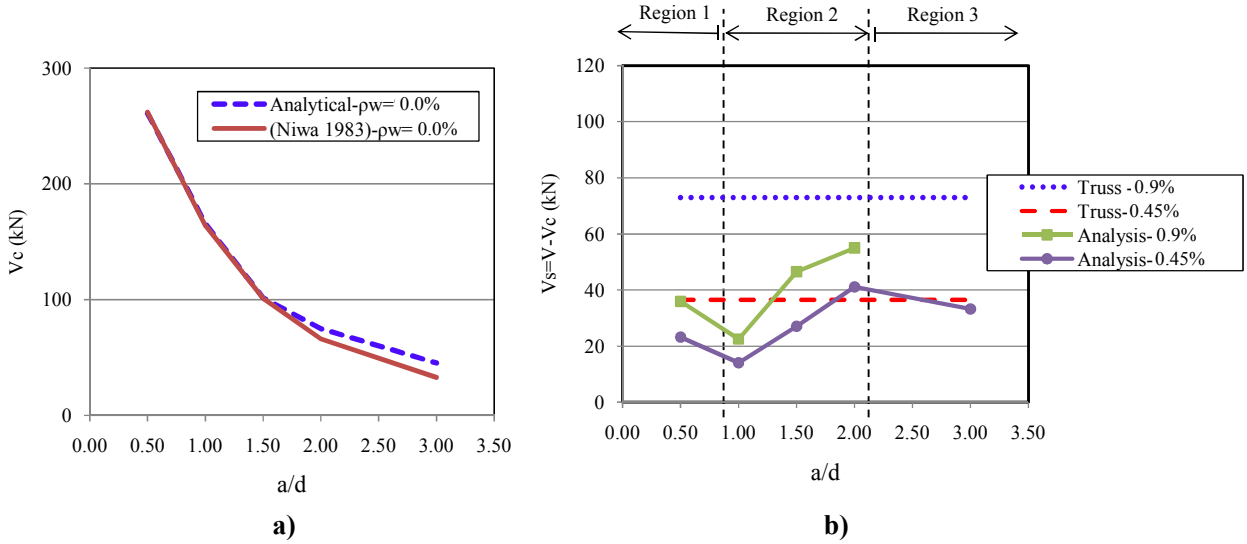

Fig. 19 Comparison of shear force.

the increase in load is not sensitive to the stirrup ratio as seen in the figure. Moreover, the crack pattern is similar in both the B3-0.5 and B3-0.5-VS cases as discussed in Section 4, that is, the arrangement of the stirrups does not affect the crack pattern.

Figures 21.a and **21.b** show the principal stress distribution on the middle longitudinal beam section and on the cross section at the middle of the shear span at the peak loads for B3-0.5 and B3-0.5-VS, respectively. The maximum stress range is set to 32.5 MPa (1.3*fc*'). The distribution is similar for the B3-0.5 and B3-0.5-VS specimens. High stress concentration occurs along the strut in both cases, as seen in the figure. Therefore, it is confirmed that the load is mainly transferred from the bearing plates to the support based on the strut action by an effective strut.

In order to investigate the effect of stirrups clearly, the stress difference between B3-0.5-VS and B3-0.5 is given in **Fig. 21.c**. The figure was obtained by subtracting the principal stress values of B3-0.5 from B3-0.5-VS at the peak load. That is, the figure demonstrates the increase of the principal stress caused by stirrups only. As seen in **Fig. 21.c**, the increase of stress is observed only near the sides of the bearing and support plates, where the localization behavior occurs in deep beams. The behavior is confirmed by the comparison of cross-sectional stress distribution between B3-0.5 and B3-0.5-VS (see **Fig. 21.c**). The stress increase may contribute to the increase of maximum load.

Figure 22 shows the comparison of the shear crack widths between B3-0.5 and B3-0.5-VS. As seen in the figure, the crack widths are limited and the growth rate is relatively small for both cases. Moreover, stirrups do not yield in the *a/d*=0.5 case as discussed in Section 4. That is, the effect of stirrups on the crack width is not significant and therefore stirrups do not contribute to the shear strength mechanism.

Figure 23 shows 3-D deformed shapes for the B3-0.5

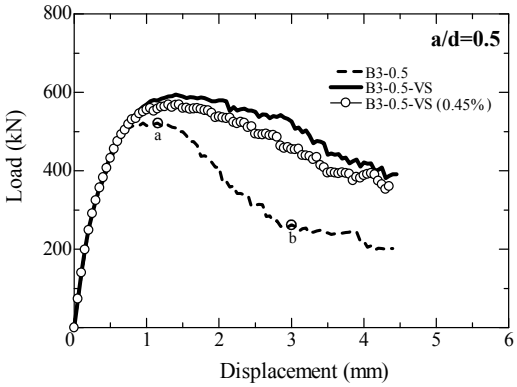

Fig. 20 Load-displacement curve (a/d=0.5).

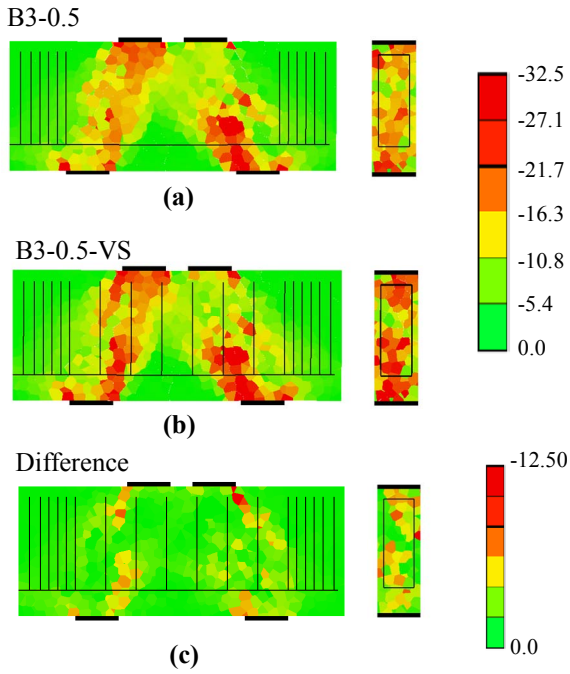

Fig. 21 Stress distribution (a/d=0.5).

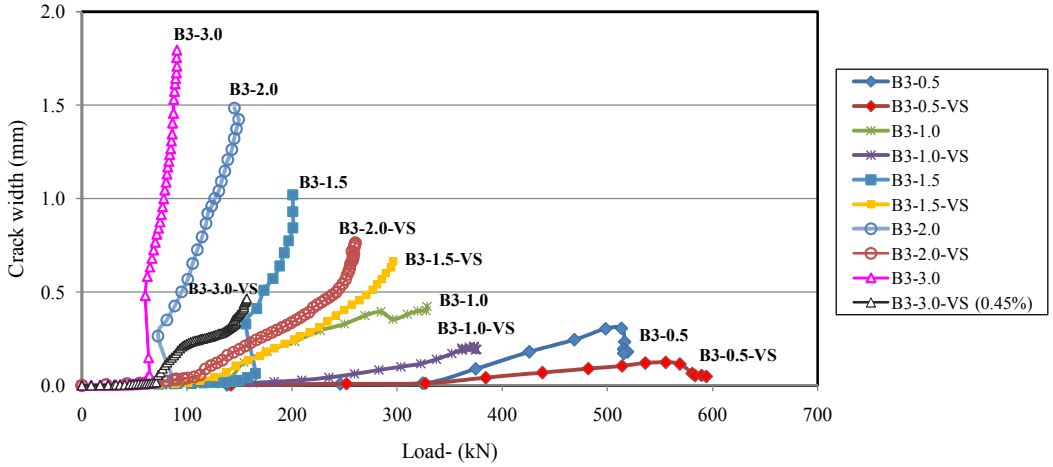

Fig. 22 Comparison of crack width.

specimen at the peak (a) and a post-peak load (b), which are labeled in **Fig. 20**. At the peak load (a), concrete spalling is observed within the strut and a large amount of concrete spalling occurs in the post-peak region (b). It is understood that in the *a/d*=0.5 case, lateral deformation rather than vertical deformation is dominant. The stirrup resists against the lateral deformation as discussed above and provides confinement within the strut. Therefore, the increase in load and ductility in the beams with stirrup is caused by the confinement effect due to the stirrups rather than the stirrup effect along the vertical direction. The beam effect represented by the B region does not occur in the *a/d*=0.5 case. Therefore, the entire beam is considered as a single D region. In Region 1, the confinement effect of stirrups is dominant.

5.2 Region 3

5.2.1 *a/d*=3.0 case

Figure 24 shows the load displacement curves for the B3-3.0 and B3-3.0-VS (0.45%) specimens. The load and ductility significantly increase in the B3-3.0-VS (0.45%) case as expected. **Figure 25** shows a comparison of the crack pattern at the peak load. The two figures are magnified by a factor of 20. As seen in **Fig. 25.a**, the damage is localized on one main diagonal crack, which leads to a diagonal shear failure in the B3-3.0 case. On the other hand, many shear cracks form in the B3-3.0-VS (0.45%) specimen (see **Fig. 25.b**). Moreover, the effect of stirrups on the crack width is also confirmed by **Fig. 22**. That is, the crack width significantly decreases due to the stirrup arrangement.

Figures 26.a and **26.b** shows the principal stress distribution along the middle longitudinal section of the beam for the B3-3.0 and B3-3.0-VS (0.45%) specimens, respectively. In the B3-3.0 case, a stress flow is observed from the bearing plates to supports. On the other hand, in the B3-3.0-VS (0.45%) case, stress is distributed in a wide area and the clear difference of stress distribution is observed due to the effect of stirrups.

The difference of principal stress between B3-3.0-VS (0.45%) and B3-3.0 specimens is given in **Fig. 26.c**. The

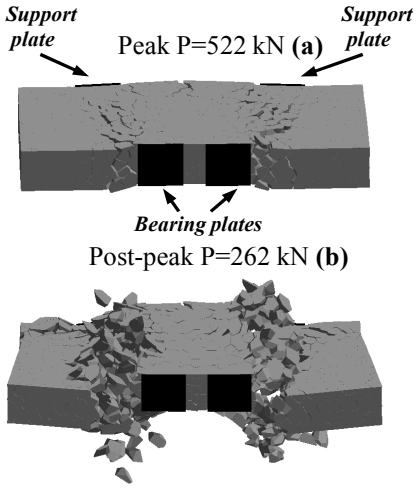

Fig. 23 3-D deformed shapes (a/d=0.5).

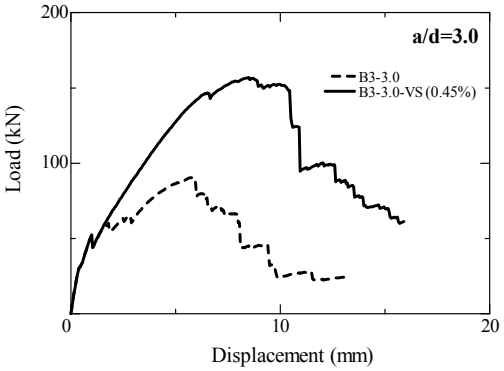

Fig. 24 Load displacement curve (a/d=3.0).

beam effect caused by the stirrups in slender beams can be investigated clearly from the figure. The stress flow can be seen to be based on the truss analogy. That is, a compressive top chord and diagonal struts appear, and this is superposed with the stress distribution of the no

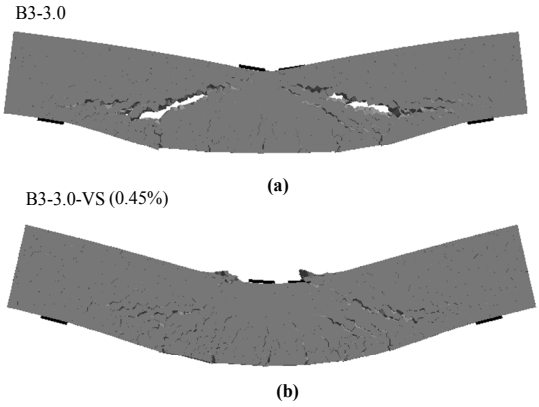

Fig. 25 Crack pattern at peak load.

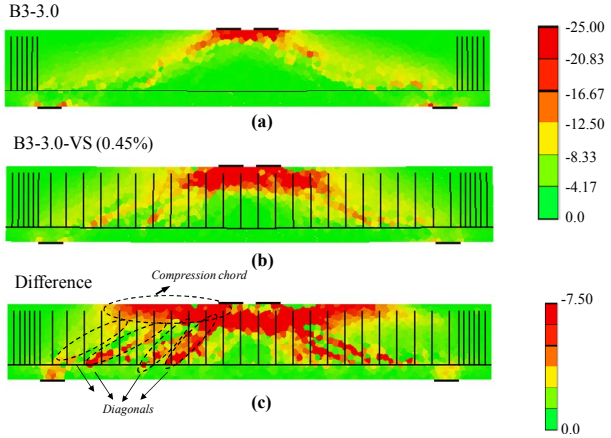

Fig. 26 Stress distribution (a/d=3.0).

stirrup case. Therefore, the beam action (B region) is observed from a distance from the bearing and support plates. It is confirmed that the B and the D regions are formed separately in slender beams as defined in the ACI-318-05 Code.

These results confirm the design concept based on the truss analogy for slender beams given in the JSCE 2007 and ACI-318-05 Codes, where the shear strength of the beam can be calculated as $V=Vc+Vs$. That is, the concrete contribution (Vc) remains after occurrence of a diagonal crack and the stirrup contribution (Vs) is superposed.

5.3 Region 2

The load displacement curves of the a/d=1.0, 1.5 and 2.0 cases are given in **Figs. 27**, **28** and **29**, respectively. In all cases, an increase in load as well as ductility is observed in the beams with stirrups. The increase rate increases with larger a/d ratios that were already confirmed in **Fig. 19.b**. Moreover, the load displacement curves are more sensitive to the change of stirrup ratio for larger a/d cases.

Strain of stirrups for a/d=1.0, 1.5 and 2.0 has already been discussed in Section 4. A similar behavior is also observed in this section. In the a/d=1.0 case, only one of the stirrups within the shear span reaches yielding strain

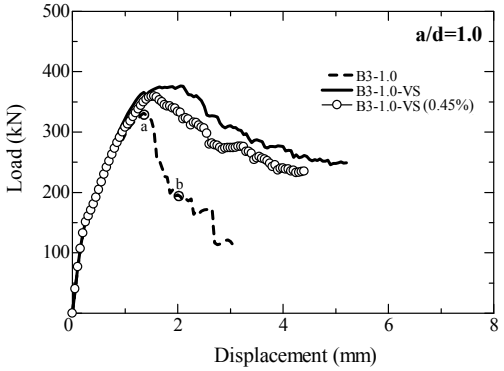

Fig. 27 Load-displacement curve (a/d=1.0).

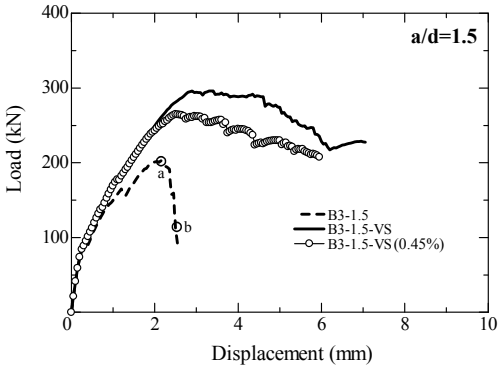

Fig. 28 Load-displacement curve (a/d=1.5).

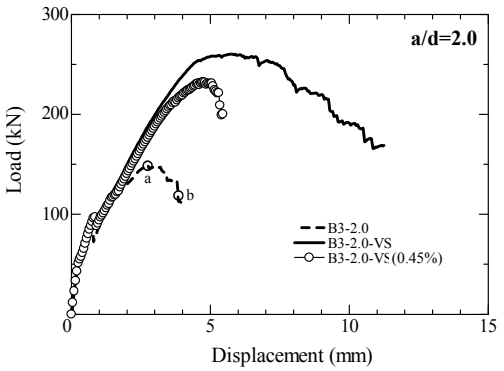

Fig. 29 Load-displacement curve (a/d=2.0).

near the peak load. On the other hand, two stirrups in the a/d=1.5 case and three stirrups in the a/d=2.0 case yield before the peak load. This confirms that the stirrup effect increases for larger a/d ratios.

The comparison of the crack pattern for a/d=1.0, 1.5 and 2.0 was also given in Section 4. In the a/d=1.0 case, the number of cracks slightly increases due to the stirrups. For the a/d=1.5 and 2.0 cases, the number of cracks remarkably increases in the beams with stirrups compared to the no stirrup cases, which provides more energy absorption that leads to increases in load and ductility.

The comparison of the shear crack widths between specimens with and without stirrups for a/d=1.0, 1.5 and 2.0 are given in **Fig. 22**. In the a/d=1.0 case, the crack widths are small and the growth rate is also limited for

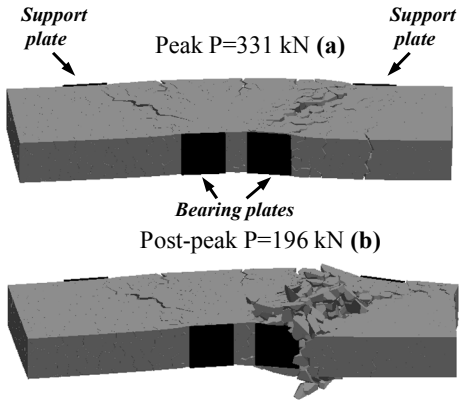

Fig. 30 3-D deformed shape (a/d=1.0).

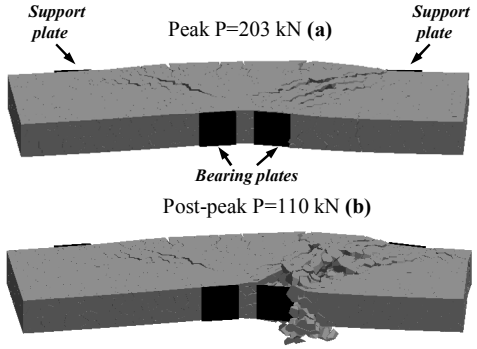

Fig. 31 3-D deformed shape (a/d=1.5).

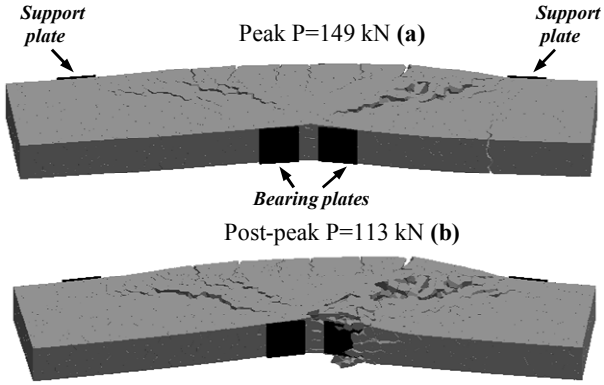

Fig. 32 3-D deformed shape (a/d=2.0).

both the B3-1.0 and B3-1.0-VS cases. That is, the effect of stirrups on the crack development is limited. For the *a/d*=1.5 case, the crack width and the growth rate are high for the B3-1.5 specimen. On the other hand, the crack widths and growth rate decrease significantly in the B3-1.5-VS case, which shows the effectiveness of stirrups for preventing crack development. Similarly with the B3-1.5 specimen, the crack width and the growth rate are significantly high for the B3-2.0 specimen while the crack width and growth rate decrease significantly in the B3-2.0-VS case. That is, stirrups effectively contribute to the shear resistance mechanism.

3-D deformed shapes of B3-1.0, B3-1.5 and B3-2.0

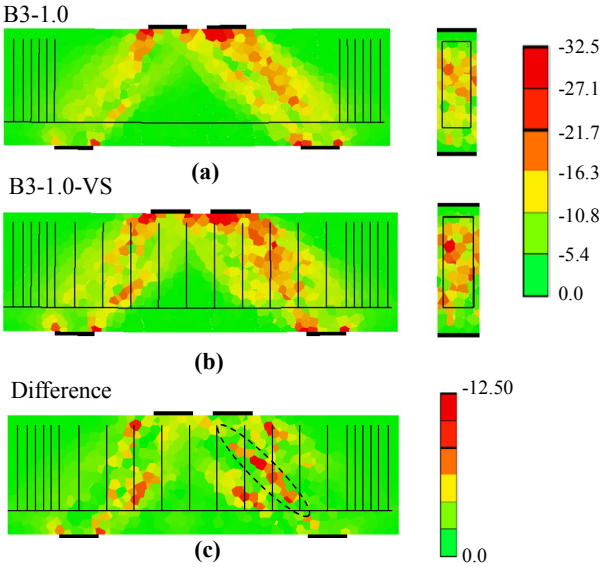

Fig. 33 Stress distribution (a/d=1.0).

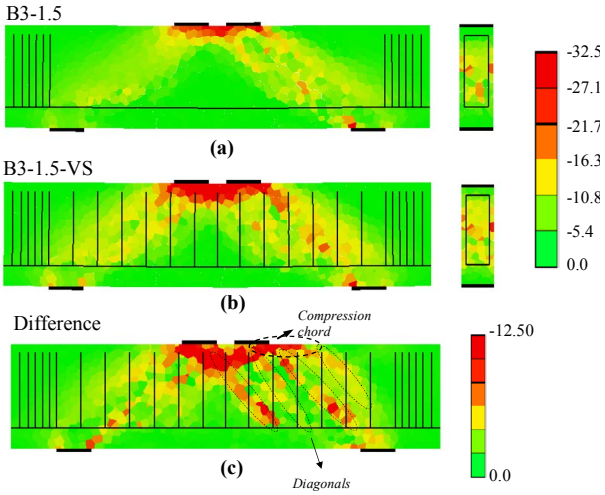

Fig. 34 Stress distribution (a/d=1.5).

specimens for the peak and a post-peak load are given in **Figs. 30**, **31** and **32**, respectively. In the *a/d*=1.0 case, concrete spalling is observed at the peak load (a) and it increases in the post peak (b). However, the amount of spalling is smaller compared to the B3-0.5 case. On the other hand, lateral deformation is observed only near the bearing plate in the B3-1.5 specimen and it is not dominant in terms of behavior. In the B3-2.0 specimen, lateral deformation is not notable as seen in the figure. Therefore, it may be noted that stirrups are effective for the shear resistance mechanism in Region 2 and the confinement effect with lateral deformation remarkably decrease with increases in the *a/d* ratio.

The principal stress distribution for the *a/d*=1.0, 1.5 and 2.0 cases are shown in **Figs. 33**, **34** and **35**, respectively. **Figures 33.a** and **33.b** shows the stress distribution for B3-1.0 and B3-1.0-VS specimens. The load is transferred from bearing plates to support by a continuous strut as seen in the figures. In the B3-1.0-VS case,

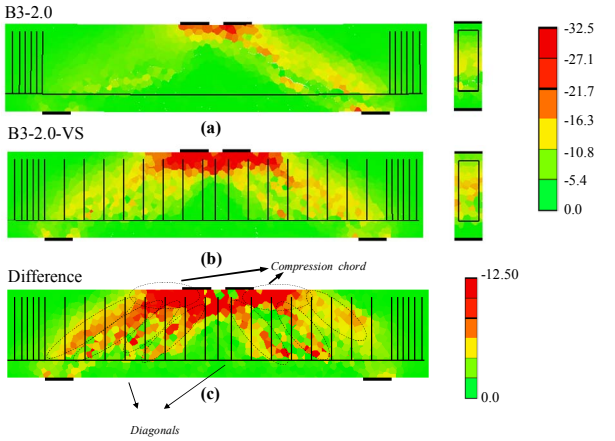

Fig. 35 Stress distribution (a/d=2.0).

the strut width slightly increases due to the stirrups.

The stress distribution for the B3-1.5 and B3-1.5-VS specimens is given in **Figs. 34.a** and **34.b**, respectively. The stress concentration occurs between bearing plates due to bending effects. A weaker strut behavior is observed and the stress values within the strut are smaller for both the B3-1.5 and B3-1.5-VS specimens compared to the *a/d*=0.5 and 1.0 cases. Moreover, the strut continuity is weak near the support as seen in the figures. On the other hand, the strut width increases remarkably in the B3-1.5-VS case due to the stirrup arrangement.

Figures 35.a and **35.b** show the principal stress distribution for the B3-2.0 and B3-2.0-VS specimens. The stress concentration between bearing plates also occurs due to bending effects. Similarly with the *a/d*=1.5 case, the strut behavior is weaker compared to the *a/d*=0.5 and 1.0 cases. The strut continuity from bearing plates to support is weak especially near the support plates in both the B3-2.0 and B3-2.0-VS cases. On the other hand, the strut width increases significantly due to the stirrup arrangement.

The comparison of cross-sectional stress distribution at the mid-shear span for *a/d*=1.0, 1.5 and 2.0 cases are also shown in **Figs. 33**, **34** and **35**, respectively. In the *a/d*=1.0 case, the stress of the cross-section slightly increases in B3-1.0-VS, however the effect is smaller compared to the *a/d*=0.5 case. On the other hand, there is no high stress state and the confinement effect is not observed in the B3-1.5-VS and B3-2.0-VS cases since lateral deformation is not dominant. Therefore, these results also confirmed that stirrups do not work for confinement in Region 2.

The difference of principal stress between specimens with and without stirrups for the *a/d*=1.0, 1.5 and 2.0 cases are given in **Figs. 33.c**, **34.c** and **35.c**, respectively, in order to investigate the occurrence of the B and D regions and clarify the load carrying mechanism. **Figure 33.c** shows the stress difference for the *a/d*=1.0 case. In the main strut direction, a sub-strut is formed that contributes to strut action, which is also confirmed by the stress increase near the mid-height cross-section (see **Fig. 33.b**). However, a compression chord on the top of the beam does not occur. That is, the beam effect and a similarity with truss analogy do not appear clearly. Therefore, no B region occurs and the entire beam should be considered as a single D region in the *a/d*=1.0 case.

The difference of stress for the *a/d*=1.5 and 2.0 cases are given in **Figs. 34.c** and **35.c**. The difference in the *a/d*=1.5 and 2.0 cases are similar, which are also similar with the *a/d*=3.0 case. As seen in the figures, sub-struts are formed continuously from the top of the beam to the longitudinal reinforcement level, and a compression chord occurs on the top of the shear span, which is similar with the truss analogy. Therefore, stirrups also contribute to load transfer by occurrence of the beam effect. That is, the beam action (B region) is also effective for the shear failure mechanism as well as the strut action. Moreover, the truss analogy is more dominant in the behavior than the strut action. As a result, the B and the D regions are superposed in the *a/d*=1.5 and 2.0 cases. This result is different from the ACI 318-0.5 Code, in which the entire member is considered as a single D region for deep beams.

6. Results and discussion

(1) A series of beams having *a/d*=0.5 to 2.0 were tested and analyzed in order to investigate the applicability of 3-D RBSM on deep beams with stirrups. The load displacement curves, the crack pattern and the strain of stirrups were compared between the experimental and the analytical results and significantly good agreement was found. It was shown that 3-D RBSM can simulate local and micro behavior as well as macro behavior. Therefore, the applicability of the analytical method was confirmed.

(2) Based on the analytical results, the beams with *a/d*=0.5 to 3.0 were classified into three regions considering the effect of stirrups on the shear failure mechanism and load carrying capacity. Region 1 includes the beams with *a/d*=0.5, in which 3-D effects and lateral deformation rather than vertical deformation are dominant in terms of shear strength. There is no effect of stirrups along the vertical direction. The load increases due to the confinement effect provided by the stirrups. In this case, the strut action is dominant in terms of behavior and the entire member is considered as a single D region.

(3) Region 3 includes the slender beams with *a/d*=3.0. By comparing the stress distribution between the beams with and without stirrups, the occurrence of compression chords and compression diagonals due to stirrups was demonstrated, which agrees with the truss analogy. The fact that the B and D regions are formed separately as defined in the ACI 318-0.5 Code for slender beams was clarified. It was confirmed that *Vs* can be superposed with *Vc*

to obtain the shear strength.

(4) Region 2 includes the beams with *a/d*=1.0, 1.5 and 2.0. In this region, stirrups are effective along the vertical direction. In the *a/d*=1.0 case, lateral deformation is also observed, however it is less effective compared to the *a/d*=0.5 case. There is limited effect of the stirrups in this case and the stirrups contribute to strut action, which is dominant in terms of behavior. Therefore, the entire member should be considered as a single D region for the *a/d*=1.0 case. On the other hand, the effect of stirrups is remarkable in the *a/d*=1.5 and 2.0 cases. The load as well as the ductility increase significantly. The occurrence of compression chords and compression diagonals due to stirrups was also observed in this case. That is, the mechanism of beams with stirrups shows similar behavior with the truss analogy. Both strut action and truss effect provided by stirrup contribute to the load carrying mechanism. Moreover, the truss analogy is more dominant in terms of behavior than the strut action. As a result, the B and the D regions are superposed in the *a/d*=1.5 and 2.0 cases. This result is different from the ACI 318-0.5 Code, in which the entire member is considered as a single D region for deep beams.

(5) For future study, these results should be extended and generalized for deep beams by evaluation of a wider range of specimens with various parameters such as size and stirrup ratio (%).

References

ASCE-ACI Committee 445, (1998). "Recent approach to shear design of structural concrete." *Journal of Structural Engineering* 124(12), 1375-1417.

ACI Committee 318, (2005). "*Building code requirements for structural concrete (ACI 318-05) and commentary (ACI 318R-05)*". Farmington Hills (MI): American Concrete Institute.

Ashour, A. F., (2000). "Shear capacity of reinforced concrete deep beams." *Journal of Structural Engineering*, ASCE, 126, 1045-1052.

Ashour, A. F., Alvarez, L. F. and Toropov, V. V., (2003). "Empirical modeling of shear strength of RC deep beams by genetic programming." *Computers and Structures*, 81(5), 331-338.

Averbuch, D. and de Buhan, P., (1999). "Shear design of reinforced concrete deep beams: a numerical approach." *Journal of Structural Engineering*, ASCE, 125(3), 309-318.

Bolander, J. E., Hong, G. S. and Yoshitake, K., (2000). "Structural concrete analysis using Rigid-Body-Spring Networks." *Computer-Aided Civil and Infrastructure Engineering*, 15, 120-133.

Bolander, J. E. and Hong G. S., (2002). "Rigid-Body-Spring Network modeling of prestressed concrete members." *ACI Structural Journal*, 99(5), 595-604.

Comite Euro-International du Beton, (1990). "*CEB-FIB model code 1990 first draft.*" CEB, Paris.

Gedik, Y. H., Nakamura, H., Yamamoto, Y. and Kunieda, M., (2010). "Analyses of pre- and post-peak behavior of deep beams failed in shear using 3-D-RBSM." In: Oh B. H, editor. *Proceedings of the 7th International Conference on Fracture Mechanics of Concrete and Concrete Structures*, Jeju, 23-28 May, 493-500.

Gedik, Y. H., Nakamura, H., Yamamoto, Y. and Kunieda, M., (2011). "Evaluation of three-dimensional effects in short deep beams using a rigid-body-spring-model." *Cements & Concrete Composites*, 33, 978-991.

JSCE, (2002). "*The standard specifications for concrete structures.*" Tokyo: Japan Society of Civil Engineers.

JSCE, (2007). "*Standard specifications for concrete structures*." Tokyo: Japan Society of Civil Engineers. (In Japanese).

Kuo, W. W., Cheng, T. J. and Hwang, S. J., (2010). "Force transfer mechanism and shear strength of reinforced concrete beams." *Engineering Structures*, 32, 1537-1546.

Kawai, T., (1978). "New discrete models and their application to seismic response analysis of structures." *Nuclear Engineering and Design*, 48, 207-229.

Kosa, K., Umemoto, Y., Nishioka, T. and Kobayashi, H., (2005). "Experimental studies on failure mode in the deep beam." *Journal of Structural Engineering*, JSCE 51A,1283-1290. (In Japanese).

Kosa, K., Wakiyama, T., Nishioka, T. and Kobayashi, H., (2006). "Effect of shear span ratio on the fracture of deep beams." *Doboku Gakkai Ronbunshuu E*, 62(4), 798-814. (In Japanese).

Mau, S. T. and Hsu T. T. C., (1989). "Formula for the shear strength of deep beams." *ACI Structural Journal*, 86(5), 516–523.

MacGregor, J. G., (1997). "*Reinforced concrete: mechanics and design.*" (3rd ed.), Prentice Hall, Upper Saddle River, NJ.

Mau, S. and Hsu, T. T. C., (1987). "Shear strength prediction for deep beams with web reinforcement." *ACI Structural Journal*, 84, 513-523.

Mörsch, E., (1920). "*Der Eisenbetonbau-seine Theorie und Anwendung (Reinforced concrete construction – Theory and application).*" 5th Ed., *Wittwer*, Stuttgart, Vol. 1, Part 1.

Mörsch, E., (1922). "*Der Eisenbetonbau-seine Theorie und Anwendung (Reinforced concrete construction – Theory and application).*" 5th Ed., Wittwer, Stuttgart, Vol. 1, Part 2

Niwa, J., (1983). "Equation for shear strength of reinforced concrete deep beams based on FEM analysis." *Proceedings of JCI 2nd Colloquium on Shear Analysis of RC Structures*, 119-126.

Nagai, K., Sato, Y. and Ueda, T., (2005). "Mesoscopic simulation of failure of mortar and concrete by 3D RBSM." *Journal of Advanced Concrete Technology*, JCI, 3(3), 385-402.

Ritter W., (1899). "Die Bauweise Hennebique." *Schweizerische Bauzeitung*. 33, 59-61.

Rogowsky, D. M., MacGregor, J .G. and Ong, S. Y., (1986). "Test of reinforced concrete deep beams." *ACI Structural Journal*, 83, 614-623.

Smith, K. N. and Vantsiotis, A. S., (1982). "Shear strength of deep beams." *ACI Structural Journal*, 79, 201–213.

Suga, M., Nakamura, H., Higai, T. and Saito, S., (2001). "Effect of bond properties on the mechanical behavior of RC beams." *Proceedings of Japan Concrete Institute*, 23(3), 295-300 (In Japanese).

Schlaich, J., Schäfer, K. and Jennewein, M., (1987). "Toward a consistent design of structural concrete." *PCI Journal*, Special Report, 32(3).

Saito S., (1999). "*Fracture analyses of structural concrete using spring networks with random geometry.*" PhD thesis. Fukuoka, Kyushu University.

Sanad, A. and Saka, M. P., (2001). "Prediction of ultimate shear strength of reinforced-concrete deep beams using neural networks." *Journal of Structural Engineering*, ASCE, 127(7), 818-828.

Salamy, M. R., Kobayashi, H. and Unjoh, S., (2005). "Experimental and analytical study on RC deep beams." *Asian Journal of Civil Engineering (Building and Housing)*, 6(5), 409-421.

Saito, S. and Hikosaka, H., (1999). "Numerical analysis of reinforced concrete structures using spring network model." *Journal of Materials, Concrete Structures and Pavements*, JSCE, No. 627/V-44, 289-303.

Tan, K. H., Kong, F. K., Teng, S. and Weng, L. W., (1997). "Effect of web reinforcement on high strength concrete deep beams." *ACI Structural Journal*, 94(5), 572-582.

Tanimura, Y., Sato, T., Watanebe, T. and Matsuoka, S., (2004). "Shear strength of deep beams with stirrups." *Journal of Materials, Concrete Structures and Pavements*, 2004-05 No.760 V-63. (In Japanese).

Tan, K. H. and Lu, H. Y., (1999). "Shear behavior of large reinforced concrete deep beams and code comparisons." *ACI Structural Journal*, 96(5), 836-845.

Tang, C. Y. and Tan, K. H., (2004). "Interactive mechanical model for shear strength of deep beams." *Journal of Structural Engineering*, ASCE, 130(10), 1534-1544.

Wang, W., Jiang, D. and Hsu, C. T., (1993). "Shear strength of reinforced concrete deep beams." *Journal of Structural Engineering*, ASCE, 119(8), 2294-2312.

Yamamoto, Y., Nakamura, H., Kuroda, I. and Furuya, N., (2008). "Analysis of compression failure of concrete by three-dimensional Rigid Body Spring Model." *Doboku Gakkai Ronbunshuu*, 64(4), 612-630. (In Japanese).

Yamamoto, Y., (2010). "*Evaluation of failure behaviors under static and dynamic loadings of concrete members with mesoscopic scale modeling.*" PhD thesis, Nagoya, Nagoya University. (In Japanese).

Yang, K. H., Chung, H. S., Lee, E. T. and Eun, H. C., (2003). "Shear characteristics of high-strength concrete deep beams without shear reinforcements." *Engineering Structures*, 25(10), 1343-1352.

Zararis, P. D., (2003). "Shear compression failure in reinforced concrete deep beams." *Journal of Structural Engineering*, ASCE, 129(4), 544-553.